Int J Adv Manuf Technol (2016) 86:1895–1907
DOI 10.1007/s00170-015-8306-5

ORIGINAL ARTICLE

# Research on burr formation mechanism in metal cutting with a backup material

**Zhijie Zou**[1] · **Liangwei Liu**[1] · **Binglin Li**[1] · **Wenjun Deng**[1]

Received: 4 August 2015 / Accepted: 21 December 2015 / Published online: 12 January 2016


**Abstract** In order to investigate the mechanism of burr formation and burr minimization, experiment and finite element simulation were performed using identical backup material. The influences of backup material height and thickness on burr sizes and burr profiles were characterized. The experimental results and simulated analyses indicated that effective burr control can be achieved using appropriate selection of backup material parameters. Furthermore, the cutting forces at steady state were found to be the same with different backup material heights and thicknesses. Therefore, the proposed technique will have a wide range of application prospects saving time and cost of deburring. This may bring remarkable economical and societal benefits.

**Keywords** Metal cutting · Burr formation · Burr minimization · Backup material · Finite element simulation

## 1 Introduction

Burr formation, resulting from the plastic deformation of the workpiece, is a normal phenomenon in metal cutting process. It directly affects the machining quality and efficiency [1]. With the advancement of micro-machining technology, miniature components have been designed and created to be used in the precision engineering industry [2]. Burr formation has been a primary issue in precision engineering, especially in ultra-precision engineering field, which needs extra deburring with additional cost. Gillespie [3] and Takazawa [4] suggested that deburring greatly increases the product cost though it is an effective method to remove the burrs formed during machining. For some precision components, 30 % of the total part cost is spent on deburring operations [5]. Hence, to reduce deburring cost maintaining the accuracy of the parts, an understanding of burr formation mechanism and minimization of burrs is of utmost significance.

Numerous studies have been carried out on the burr formation process. Gillespie [5] explained the mechanism of burr formation and proposed a theoretical model of burr formation which can estimate burr characteristics. Pekelharing [6] proposed a theoretical model of negative shear angle that later became the theoretical basis of burr formation mechanism studies. Ko and Dornfeld [7] established burr formation models in orthogonal cutting, which can be used for brittle materials and ductile materials. It has been indicated that burr formation consists of three phases: initiation, development, and formation. Chern [8] further studied orthogonal cutting employing SEM micro-machining test to explore the mechanism of burr formation. It is reported that plastic bending deflection and shearing deformation of the negative deformation plane cause burr formation. Toropov et al. [9] analyzed the effects of rake angle, clearance angle, workpiece exit angle, and other cutting parameters on burr formation, and they later proposed two quantitative models of burr formation in orthogonal cutting used for both brittle and ductile

✉ Wenjun Deng
dengwj@scut.edu.cn

[1] School of Mechanical and Automotive Engineering, South China University of Technology, Wushan 381, Tianhe District, Guangzhou, Guangdong CN 510641, China

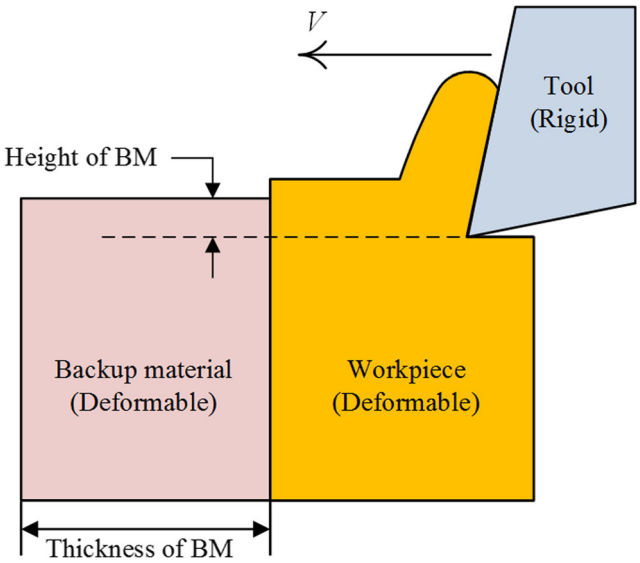


**Fig. 1** Schematic of metal cutting process with a backup material

materials [10, 11]. Except modeling orthogonal cutting, Segonds [12] proposed a burr formation model for drilling process, while Niknam et al. [13] proposed a burr thickness model for milling process. Chern [14] and Lin [15] carried out experimental work on the relationships between burr shapes and cutting parameters of aluminum alloy and stainless steel, respectively. Five different forms of burrs were discussed: knife edge, curl, wave, edge breakout, and secondary burr. Olvera [16] experimentally studied the impact of different cutting parameters on burr sizes and concluded that the depth of cut and workpiece exit angle play an important role in burr formation. Wyen et al. [17] investigated the influence of cutting edge radius on burr formation in milling titanium alloys. Wu et al. [18] experimentally analyzed the impacts of crystallographic orientation in single crystal copper and grain size in polycrystalline copper on the burr formation.

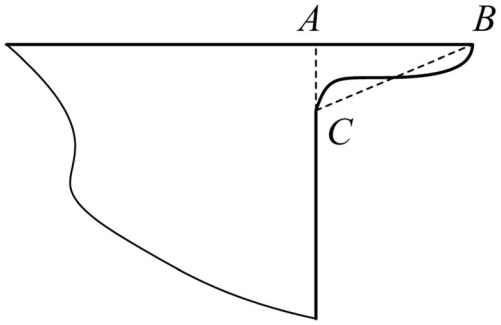


**Fig. 3** Schematic of burr area

In addition to experimental work, finite element simulation is another effective way to study the metal cutting processes [19–21], so as the burr formation processes. Some complicated models dedicated to burr formation in metal cutting have been developed in the last few decades [22–25]. Park and Dornfeld [26] built a 2D burr formation finite element model in orthogonal cutting. The influences of processing parameters were investigated, and, on the basis of stress and strain contours, four phases of burr formation were found: initiation, initial development, pivoting point, and final development stage. Deng et al. [27, 28] analyzed burr formation using finite element method and found out the relationship between cutting parameters and burr sizes. Wan et al. [29] studied the influence of processing variables on burr profiles and sizes using 3D finite element analysis model. Taguchi method [30] and artificial neural network models [31] were used to optimize the process parameters achieving the burr size minimization in drilling.

Cutting with a backup material is one of the most efficient methods to minimize the burr size. Based on finite element simulations, Park [32] explored burr minimization mechanism using backup materials. But, the proposed conditions do not agree in practice, which could cause a shock at the tool nose

**Fig. 2** Finite element model

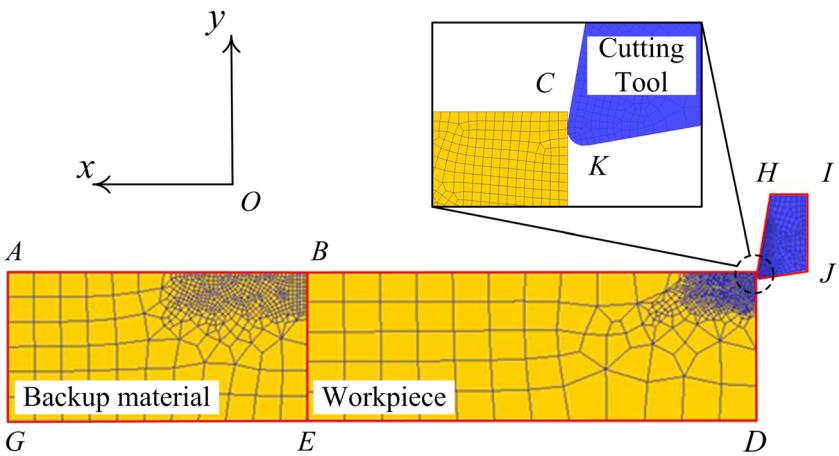

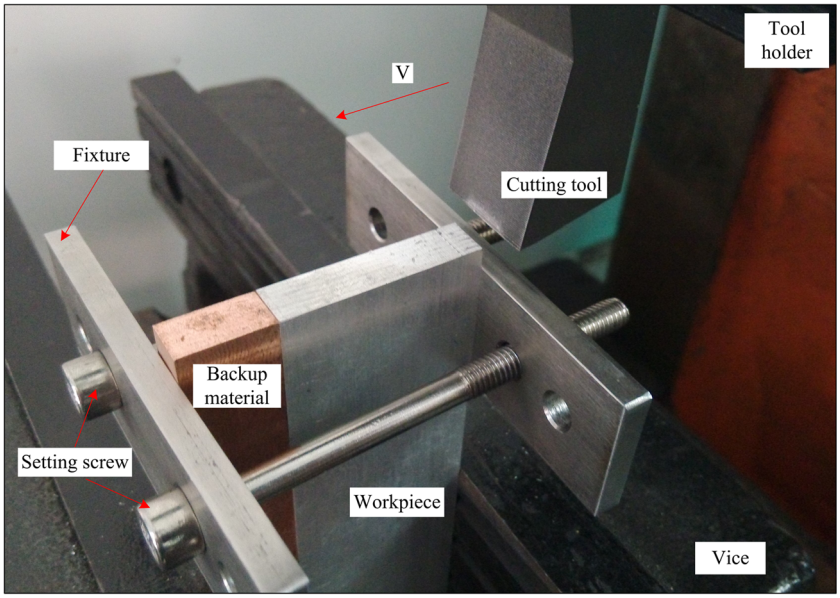


**Fig. 4** Experimental setup

and shorten tool life. Hence, additional studies are needed. However, recently, attentions were mainly paid to the impact of process variables on burr formation [9, 14–17, 26, 30, 31], while cutting process with a backup material was rarely involved. Consequently, it is essential to get a systematic and comprehensive understanding of the role of backup material in preventing burrs and prompting the production of burr-free components.

In this present work, the influence of the backup material on burr formation was experimentally studied. A modified finite element model based on the experiments was employed to study the burr minimization mechanism of backup material, so as the burr formation mechanism. The impact of backup material height and thickness was also studied. The cutting force and effective stress distribution were also analyzed.

## 2 Experimental methods

### 2.1 Finite element simulation

Cutting with a backup material can be defined as placing the backup material against the edge of the workpiece, as is shown in Fig. 1. And, there are two notable parameters, thickness and height, for backup material (BM). The thickness of BM is defined as the dimension of backup material parallel to the cutting direction, while the definition of the height of BM is the distance between top edge of backup material and machined surface of workpiece, as shown in Fig. 1. Both the workpiece and backup materials are deformable.

A commercial finite element code, DeForm-2D™, was used to perform a 2D finite element model under plane strain assumption. This model was based on a simulation for an orthogonal cutting process. In plane strain model, the workpiece and backup material can be simplified as rectangles, as shown in Fig. 2. During modeling, the cutting tool was set to be rigid and heat transferable and has much higher hardness than the workpiece. It was moveable in the horizontal direction while not vertically. A horizontal displacement boundary condition was exerted on the tool to achieve the eventual cutting process. The cutting tool cuts into the workpiece at a given speed. The workpiece and backup material were both deformable and set to be rigid plastic bodies with isotropic strain hardening. During simulation, it was expected that *C-D-E* boundary of workpiece and *G-E* boundary of backup material undergo very little deformation as the displacements of these boundaries along *x*- and *y*-direction were set to zero. The boundary *B-C* of the workpiece and boundary *G-A-B* of the backup material were unconstrained to guarantee the free formation of chips and burrs during simulation. Since large plastic deformation occurred in workpiece/backup material during metal cutting, heat generation and transfer were not negligible. The boundaries *C-D-E* of the workpiece, *G-E* of the backup material, and *H-I-J* of the cutting tool remained at room temperature, while other free surfaces of the workpiece, backup material, cutting tool, and chip were considered as heat transfer surfaces. In addition, the contacts between cutting tool and workpiece, cutting tool and backup material, and workpiece and backup material were the keys achieving realistic simulation of the metal cutting process and burr formation process. In the present study, shear friction factor used in machining was

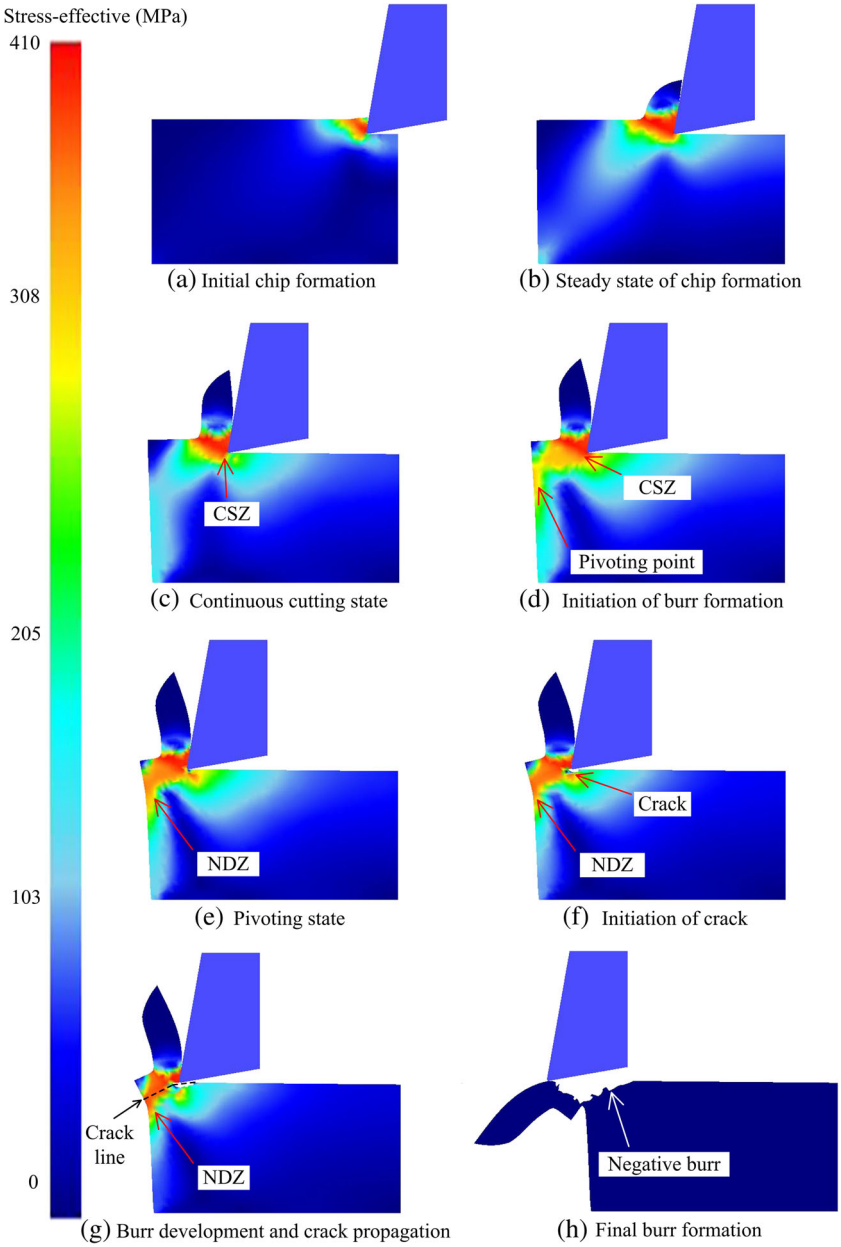


**Fig. 5** Negative burr formation process

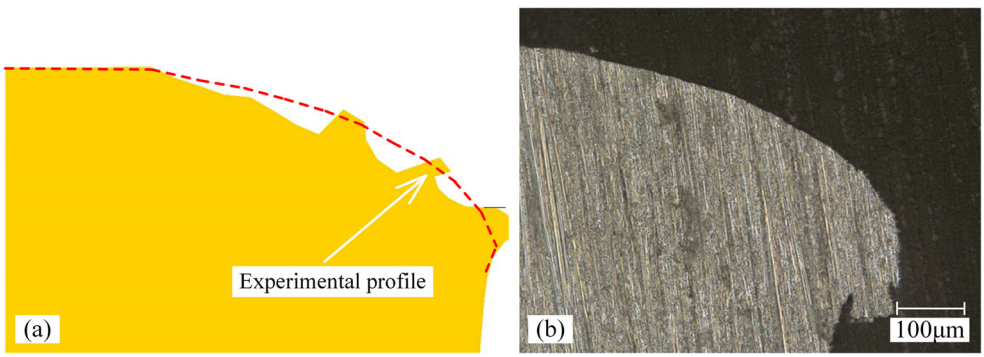


**Fig. 6** Burr morphology obtained from **a** simulation and **b** experiment

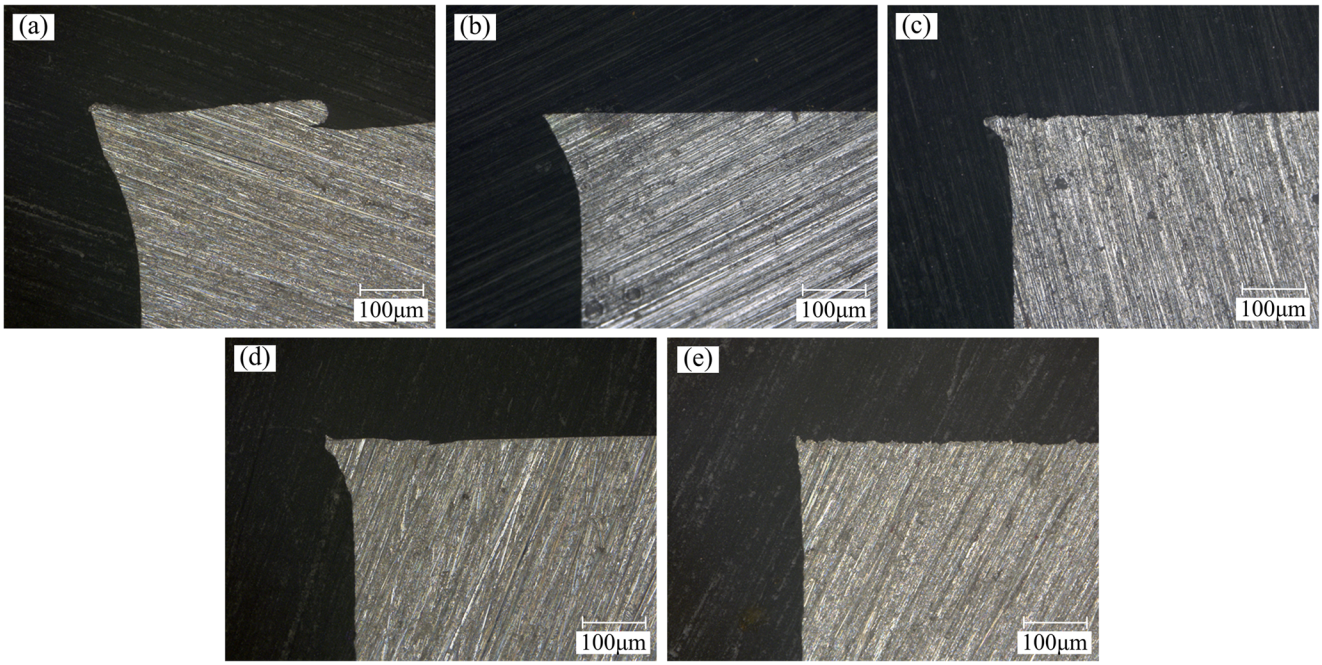


**Fig. 7** Experimental burr profiles with different thicknesses of backup material: **a** 5 mm, **b** 10 mm, **c** 15 mm, **d** 20 mm, and **e** 25 mm

0.65 and Coulomb friction factor of 0.25 was used in the contact region between workpiece and backup material.

The workpiece and backup material selected for this simulation were commercial aluminum alloy (6061-T6) with Young's modulus of 68.9 GPa. Poisson's ratio, thermal conductivity, and specific heat of aluminum alloy are 0.3, 180 W/mK, and 2.4 J/K, respectively. During metal cutting process, a complex phenomenon occurred in the deformation zone. Deformation occurred simultaneously with high strain, high strain rate, and temperature rise, which can be explained using material constitutive model. In the present simulation, Johnson-Cook model was employed, which is applicable for high strain rate conditions [33].

Normalized Cockoft and Latham's fracture criterion was used to estimate the fracture of chips and burr formation, which can be expressed using the following equation [34]:

$$\int^{\bar{\varepsilon}_f} \frac{\sigma^*}{\bar{\sigma}} d\bar{\varepsilon} = D, \tag{1}$$

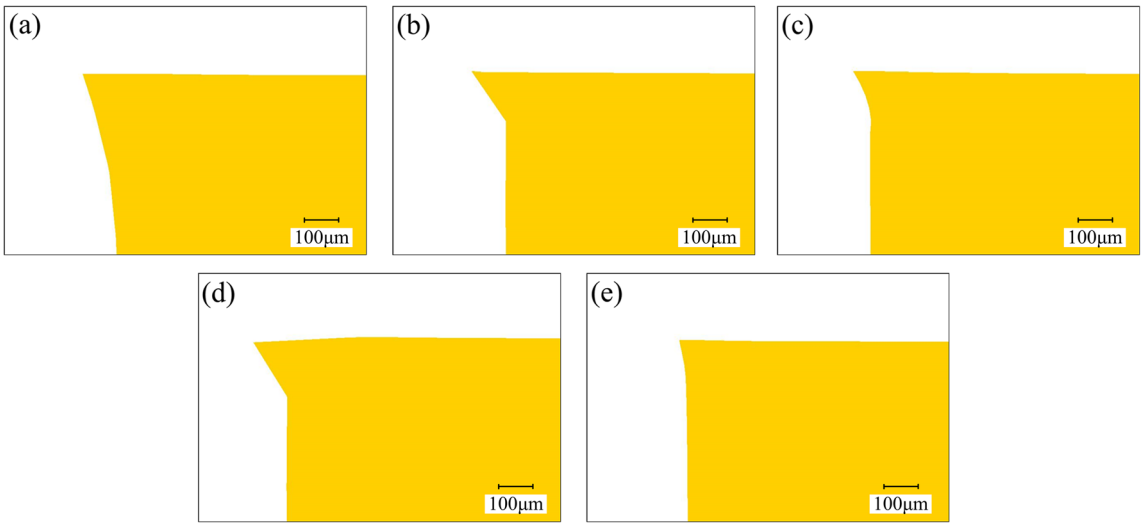


**Fig. 8** Simulated burr profiles with different thicknesses of backup material: **a** 5 mm, **b** 10 mm, **c** 15 mm, **d** 20 mm, and **e** 25 mm

where $\overline{\varepsilon}f$ is the equivalent fracture strain, $\sigma^*$ is the maximum principal stress, $\overline{\sigma}$ is the equivalent stress, $\overline{\varepsilon}$ is the effective strain, and $D$ is a material constant. The value of $D$ is generally referred to as the damage value, which is constant for a certain material and does not change with various tool materials or under different cutting conditions [35]. Deleting mesh elements is an effective way to simulate the crack initiations and propagations. Fracture initiates when four neighboring elements reach the material damage value. This value can be evaluated by a tensile test. In the present paper, the critical damage value was calculated, using trial and error, to be approximately 0.81 for aluminum alloy (6061-T6).

During finite element process, the following metal cutting parameters were chosen based on the experimental results. The depth of cut was 0.2 mm; the width of cut was 8 mm; the machining velocity was 0.11 m/s; both the rake angle and the relief angle of cutting tool were 10°; the corner radius was 0.2 mm; the ambient temperature was 20 °C. In this study, the formation of chips and burrs was supposed to be the outcomes of plastic flow and the separation of the chips from workpiece material was obtained using automatic continuous remeshing.

Burr size, such as burr height and burr root thickness, can directly be measured using finite element simulation. Burr area, the area of burrs in the cross sections, was considered to be an important parameter for analyzing the burr formation process in this study. It can be simplified as a triangle, though burrs have plenty of shapes, as shown in Fig. 3.

As for $\triangle ABC$, burr area can be calculated by

$$S = \frac{1}{2} \times AB \times AC, \tag{2}$$

where $AB$ is the burr height and $AC$ is the burr root thickness.

### 2.2 Experimental procedure

An experimental platform was set up to prepare the burr measurement samples. As shown in Fig. 4, experimental studies were performed using a universal planer (BC6063B). The cutting tool, high speed steel, was fixed by the tool holder. The workpieces and backup materials were fixed by a vice and an additional fixture. The cutting parameters used in experimental studies were consistent with the simulation studies.

The burr size and morphology of cutting samples were determined using an ultra-deep microscope (VHX-1000). All the samples were mounted using epoxy in rod shape with a diameter of 25 mm after the ultrasonic cleaning. The samples were then ground to 300 μm. At least three random cross sections of each sample were selected for the measurement, and the burr size of each cross section was measured three times. The mean burr height and burr root thickness were considered as the burr size of the samples.

## 3 Results and discussion

### 3.1 Burr formation process

In order to ascertain the impact of the backup material on burr formation, burr formation process should be studied first. The burr formation process during metal cutting, as shown in

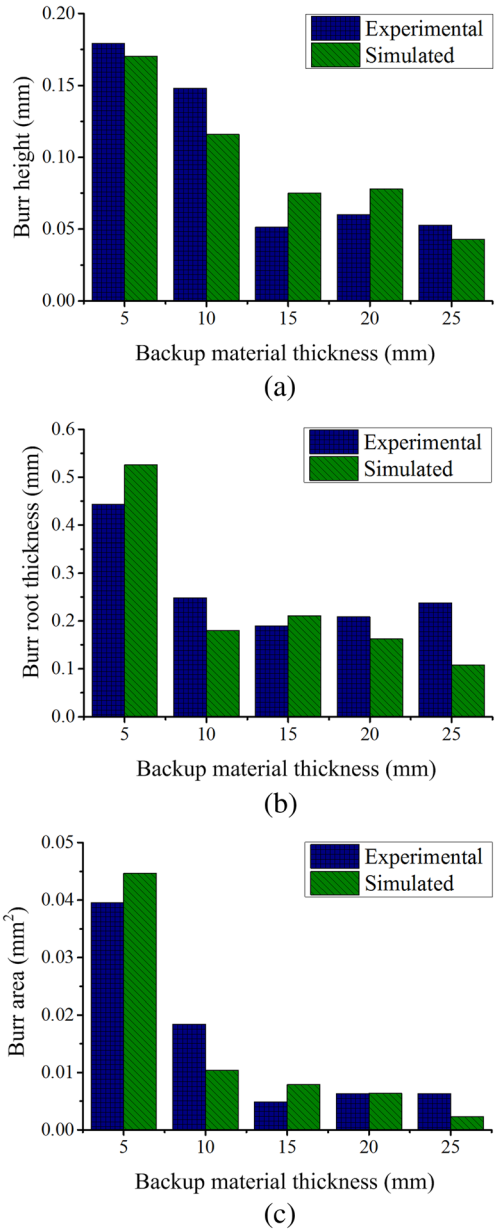


**Fig. 9** Burr sizes with different backup material thicknesses: **a** burr height, **b** burr root thickness, and **c** burr area

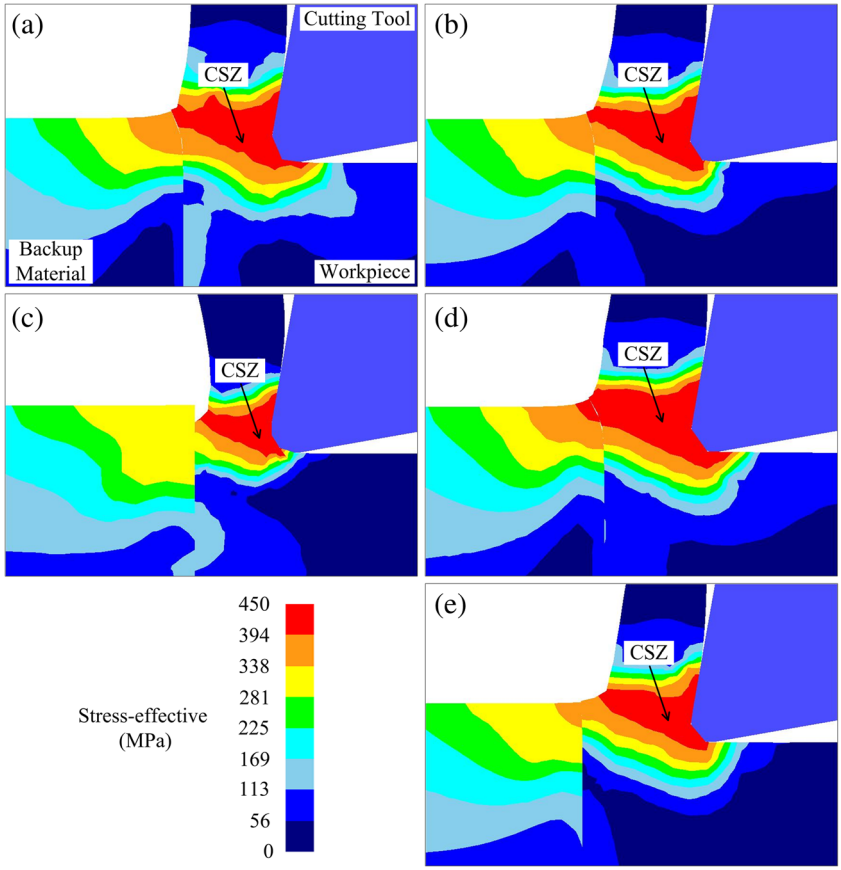


**Fig. 10** Effective stress distribution of deformation zone at pivoting state using different thicknesses of backup material: **a** 5 mm, **b** 10 mm, **c** 15 mm, **d** 20 mm, and **e** 25 mm

Fig. 5, can be divided into eight segments. When tool cut into the workpiece, initial distortion begins (Fig. 5a). Severe shearing deformation of cutting zone is revealed by the effective stress magnitude. As the tool continuously moves, a clear outline of the chips can be found and the effective stress of cutting zone commences to stabilize (Fig. 5b). Figure 5c reveals the continuous cutting state. It is evident that the effective stress and deformation behavior remain stable and are almost unaffected by the edge of workpiece. As the tool moves closer to the end of workpiece, plastic deformation zone around the primary shear zone is noticed to expand. Figure 5d indicates the initiation of burr formation where an obvious pivoting point can be seen. In addition, plastic bending deformation occurs on the edge of workpiece. It is clear that the area of plastic deformation zone around the primary shear zone expand to the edge of workpiece. Figure 5e reveals the pivoting state. Large deformation zone along the workpiece edge can easily be found, which indicates the negative deformation zone (NDZ). Pivoting point can also be observed within the large deformation zone. On the other hand, undeformed layer of the workpiece starts rotating at the corner, and thus, obvious bending of the workpiece can be found on the edge. Figure 5f shows crack initiation in workpiece where it is clear that apparent fracture can be observed at the zone near the tool nose. Similar magnitude of effective stress can be found in the cutting shear zone (CSZ)

**Table 1** Error analysis of simulation

| BM thickness (mm) | Burr height (mm) | | | Burr root thickness (mm) | | |
|---|---|---|---|---|---|---|
| | Experimental | Simulated | Error | Experimental | Simulated | Error |
| 5 | 0.1792 | 0.1697 | 0.1 % | 0.4428 | 0.5259 | 15.8 % |
| 10 | 0.1481 | 0.1162 | 21.5 % | 0.2480 | 0.1602 | 35.4 % |
| 15 | 0.0513 | 0.0750 | 31.6 % | 0.1903 | 0.2259 | 15.8 % |
| 20 | 0.0600 | 0.0783 | 23.4 % | 0.2087 | 0.1631 | 21.8 % |
| 25 | 0.0527 | 0.0429 | 18.6 % | 0.2383 | 0.1084 | 54.5 % |

and NDZ. However, fracture orientation is still not clear. Figure 5g shows the burr development and crack propagation where obvious crack line can be found. The workpiece material ruptures along the crack line direction. At this stage, the effective stress around NDZ appears to be larger than the effective stress around CSZ. Figure 5h shows the final burr formation. The chip and a portion of the workpiece material are plowed and pushed away directly by the cutting tool. Chip induced by the crack separates from the workpiece material along the crack line. Thus, some negative burrs can be observed around the corner of the workpiece. Then, the tool was unloaded, and, once the tool lost contact with the workpiece, the cutting process was accomplished. During the initial state of chip formation, steady state of chip formation, continuous cutting state, pivoting state, and initial crack state, the formation process of negative burr is similar with the positive burr [26, 27]. There is a huge difference between the two processes at the burr development and crack propagation state [26, 27]. At this stage, the normal stress of CSZ converted into tensile stress of NDZ. Thus, the largest effective stress appeared around NDZ and workpiece material fractured along the negative deformation plane. Formation of NDZ and its stress variations are considered to be the main reason of both positive and negative burr formation [7, 8]. Figure 6 shows burr morphology obtained from simulation and experiment. It is evident that experiment returned identical results predicted by simulation. It can be concluded that the simulation model of burr formation is accurate.

### 3.2 Influence of the thickness of backup materials on burr formation

Figure 7 reveals the experimental profiles of burrs with five different thicknesses of backup material. It is noted that all the burrs display positive profiles on the corner of the workpiece indicating the annihilation of negative burrs in metal cutting. Thus, potential risk of reducing surface quality and the precision is avoided. Figure 8 shows the simulated burr profiles with the same thicknesses of backup material used in the experiment. It is obvious that not only the burr profiles are very similar but also the burr sizes are found to be very close.

Figure 9 shows the burr height, burr root thickness, and burr area with five different thicknesses of backup material, respectively. The simulated and experimental values are listed in each figure. With the increase of the backup material thickness from 5 to 20 mm, it is evident that larger burr height is obtained with smaller backup thickness (Fig. 9a). Consequently, burr height became relatively small with a larger backup material thickness. Further, it is also noted that a significant drop in burr root thickness is noticed with increasing the backup material thickness from 5 to 10 mm (Fig. 9b). However, burr root thickness does not change significantly with increasing backup material thickness from 10 to 25 mm. This indicates that when the backup material thickness reaches over 10 mm, a little impact on minimizing burr root thickness is obtained. Figure 9c shows the simulated and experimental burr area with five different backup material thicknesses. It can be observed that burr area rapidly

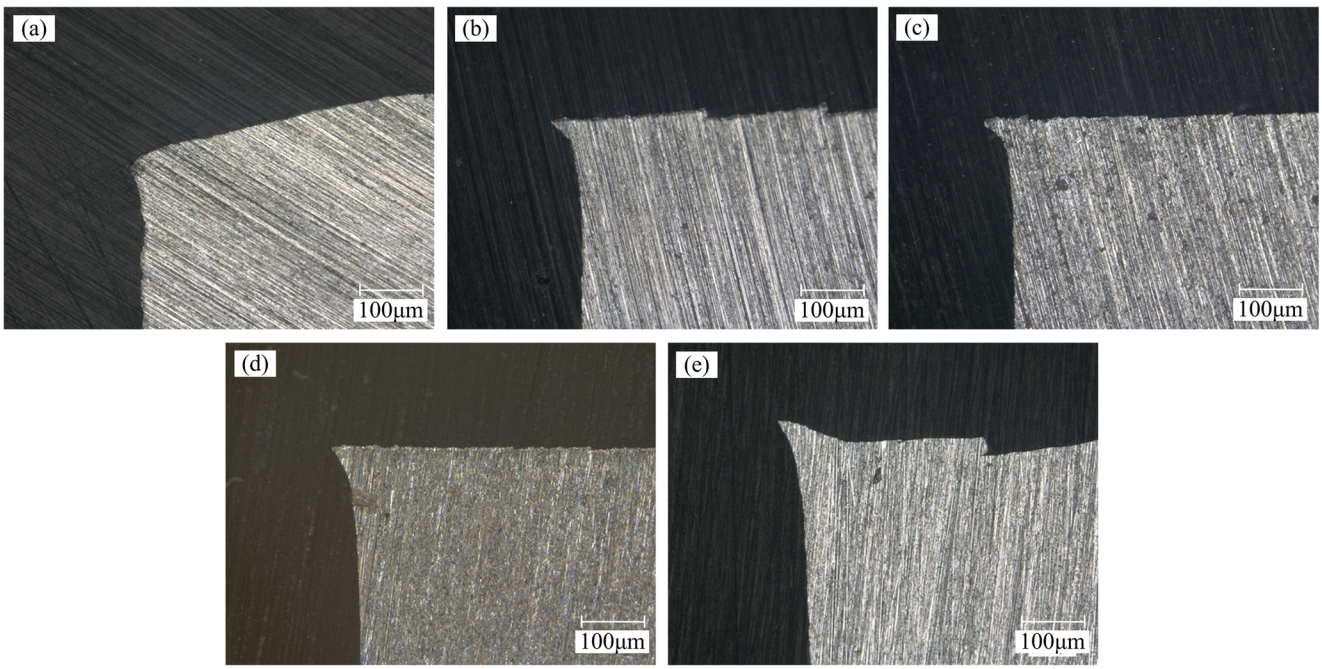


**Fig. 11** Experimental burr profiles using different heights of backup material: **a** –0.2 mm, **b** –0.1 mm, **c** 0 mm, **d** 0.1 mm, and **e** 0.2 mm

decreased with increasing backup material thickness from 5 to 10 mm. However, burr area is not reduced beyond 10-mm thickness of backup material. This is attributed to the trend of burr root thickness.

Figure 10 shows the effective stress distribution of deformation zone at pivoting state using five different backup material thicknesses. Due to the backup material, pivoting point and NDZ were inhibited and only CSZ can be found. The maximum effective stresses were 424.4, 424.6, 425.2, 424.3, and 424.7 MPa for thickness of backup material 5, 10, 15, 20, and 25 mm, respectively. It seems that the backup material thickness has little impact on the maximum effective stress at pivoting state. However, difference in burr size can be measured when cutting with different backup material thicknesses. Larger burr size was obtained for thinner backup material as support stiffness became lower. With the increase of backup material thickness, the support stiffness of backup material had been improved, and thus, the burr size reduced. It is observed that support stiffness appears to be high enough with the backup material thickness of 15 mm. Thus, it is ineffective to increase the backup material thickness beyond 15 mm. Consequently, excessively thick backup material should be avoided considering burr minimization and economic machining.

An error analysis was performed to validate the accuracy of simulation. Table 1 shows the burr size error of different backup material thicknesses. It is easy to find that the simulated value was closed to the experimental data. Generally, relative error did not exceed 25 %. Hence, simulated burr sizes and burr profiles are considered to be consistent with the experimental ones.

### 3.3 Influence of the height of backup materials on burr formation

Figure 11 shows the experimental burr profiles, and Fig. 12a–c shows the burr height, burr root thickness, and burr area using five different heights (−0.2, −0.1, 0, 0.1, and 0.2 mm) of backup material, respectively. Positive values (0.1, 0.2 mm) indicate that the top edge of backup material is higher than machined surface of workpiece. It is noted that negative burr formed when the backup material height was −0.2 mm. Further, it is apparent that the burr formation models of workpiece transformed from negative ones to positive ones with increasing the backup material height from −0.2 to −0.1 mm. However, the variation in backup material height from −0.1 to 0.2 mm slightly changed the magnitude of burr size, including burr height, burr root thickness, and burr area. But, it is quite obvious that burr size decreased with increasing backup material height. Besides, it should not be neglected that the maximum burr area appeared at the height of −0.2 mm, which means a large edge breakout area.

Figure 13 shows the effective stress distribution of deformation zone at pivoting state for five different backup material heights. The maximum effective stresses measured in simulation were 424.6, 424.7, 424.7, 423.9, and 425.2 MPa for heights of backup material −0.2, −0.1, 0, 0.1, and 0.2 mm, respectively. It is quite apparent that backup material height had little impact on the maximum effective stress at pivoting state. The difference in burr size is mainly due to the effective stress distribution. The corner of backup material acted as a

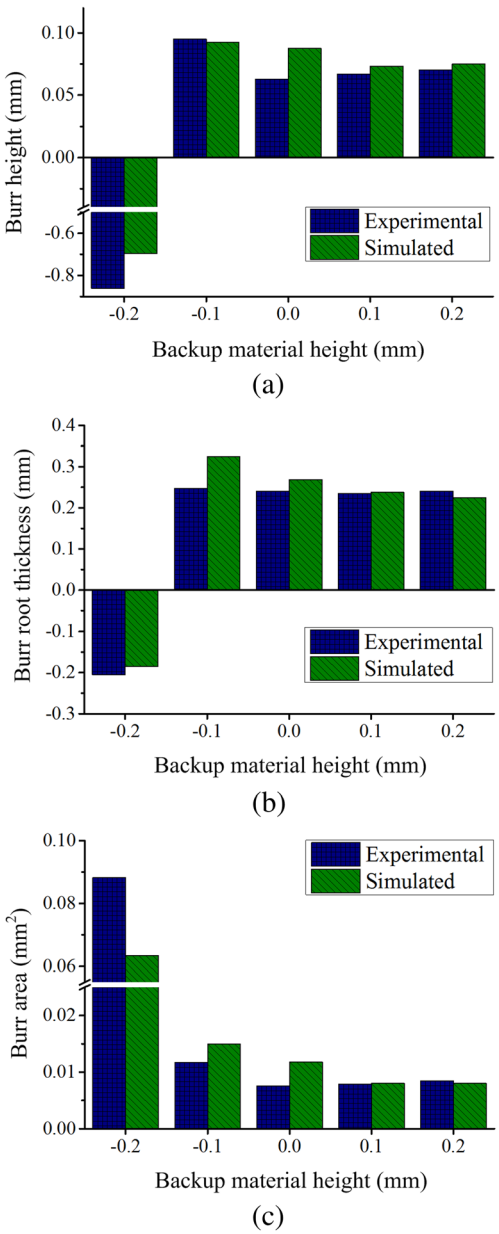


**Fig. 12** Burr sizes with different backup material heights: **a** burr height, **b** burr root thickness, and **c** burr area

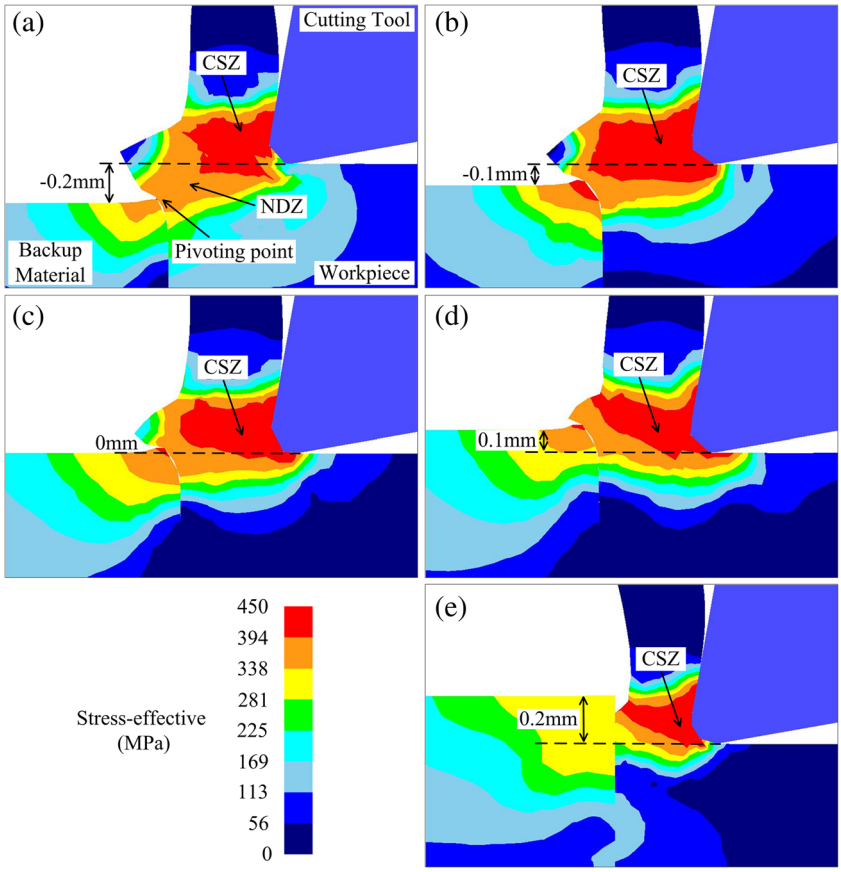


**Fig. 13** Effective stress distribution of deformation zone at pivoting state for different heights of backup material: **a** –0.2 mm, **b** –0.1 mm, **c** 0 mm, **d** 0.1 mm, and **e** 0.2 mm

pivoting point when cutting is performed with a backup material height of −0.2 mm. It contributed to the formation of large NDZ and eventually led to the formation of negative burr (Fig. 13a). On the other hand, the corner of backup material still acted as a pivoting point when cutting with a backup material height of −0.1 mm (Fig. 13b). But, no obvious NDZ can be observed. Workpiece materials flowed along the cutting direction and finally formed a positive burr. As shown in Fig. 13c–e, only CSZ can be found when backup material height varied from −0.1 to 0.2 mm. In addition, within this range (−0.1 to 0.2 mm), backup material generated sufficient support and suppressed the bending of the workpiece edge. Hence, positive burrs with similar burr sizes and burr profiles were formed. As a result, from the viewpoint of burr minimization, lower and higher backup material height should be avoided. For this study, backup material height closed to zero could be the best choice.

### 3.4 The cutting forces

The cutting force history in orthogonal cutting is shown in Fig. 14. It is noticeable that a very short time is needed to reach the steady state. At steady stage, the cutting force reached a value of about 188 N. Further, it is obvious that the cutting force curve can be divided into three regions. Region I indicates the process of cutting into the workpiece for tool. Region II is defined as the steady cutting state. Region III indicates the burr formation process. At this region III, the tool reached the workpiece edge and crack initiated

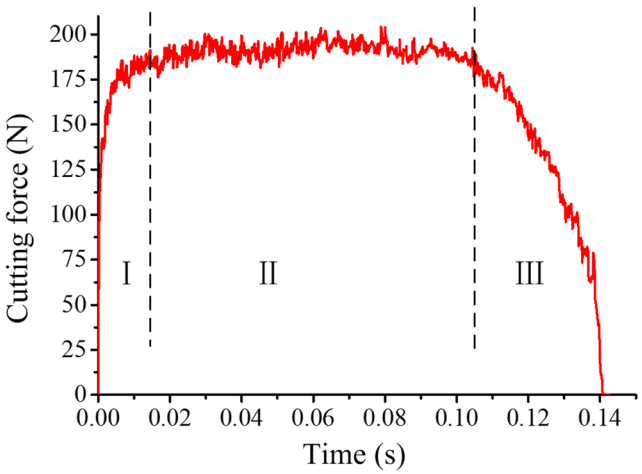


**Fig. 14** Cutting force history in orthogonal cutting

and propagated. Finally, the tool was unloaded, and the cutting force decreased to zero.

Figure 15 shows the cutting force history under five different backup material heights. In all cases, cutting force values at steady state were reached at around 188 N. No significant differences can be found. However, it can be observed that there are three regions in Fig. 15a–c while four in Fig. 15d–e. Region IV is defined as the backup material cutting state. When cutting with a backup material height of 0.1 mm, the depth of cut at backup material cutting state is 0.1 mm. And, the stable cutting force was obtained to be about 105 N. Owing to the larger depth of cut, cutting with a backup material height of 0.2 mm, the stable cutting force was found to be about 188 N. This is the same as the cutting force at steady state in region II. In addition, with a lower height of backup material, the cutting tool was unloaded along with the burr formation process, and thus, there was no backup material cutting state.

Figure 16 shows the cutting force diagram under five different backup material thicknesses. Similar force profiles and steady-state value can be observed in all cases. It is apparent that there are four regions in each figure. And, the cutting force in both cutting steady state and backup material cutting

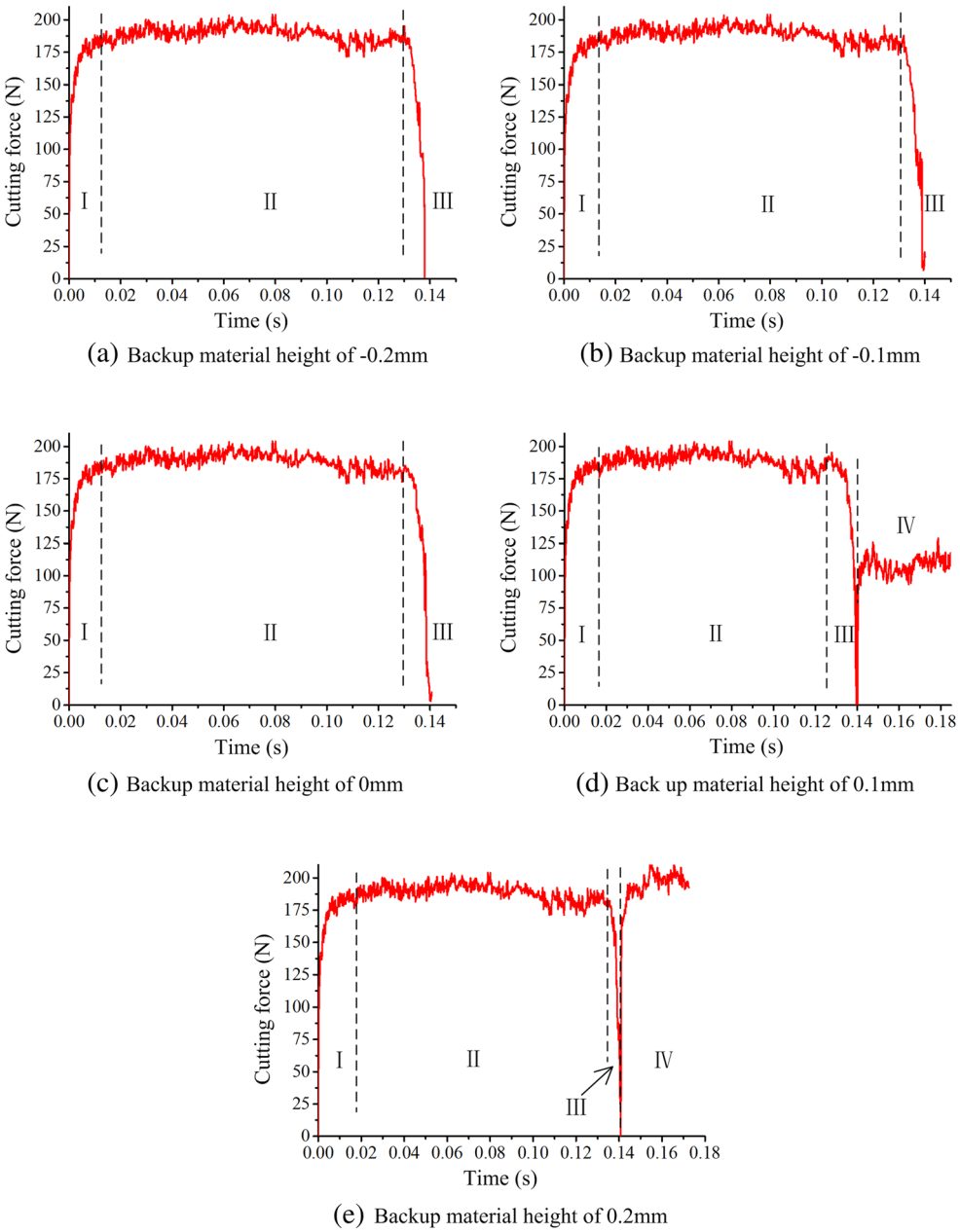


**Fig. 15** Cutting force curves under five different backup material heights

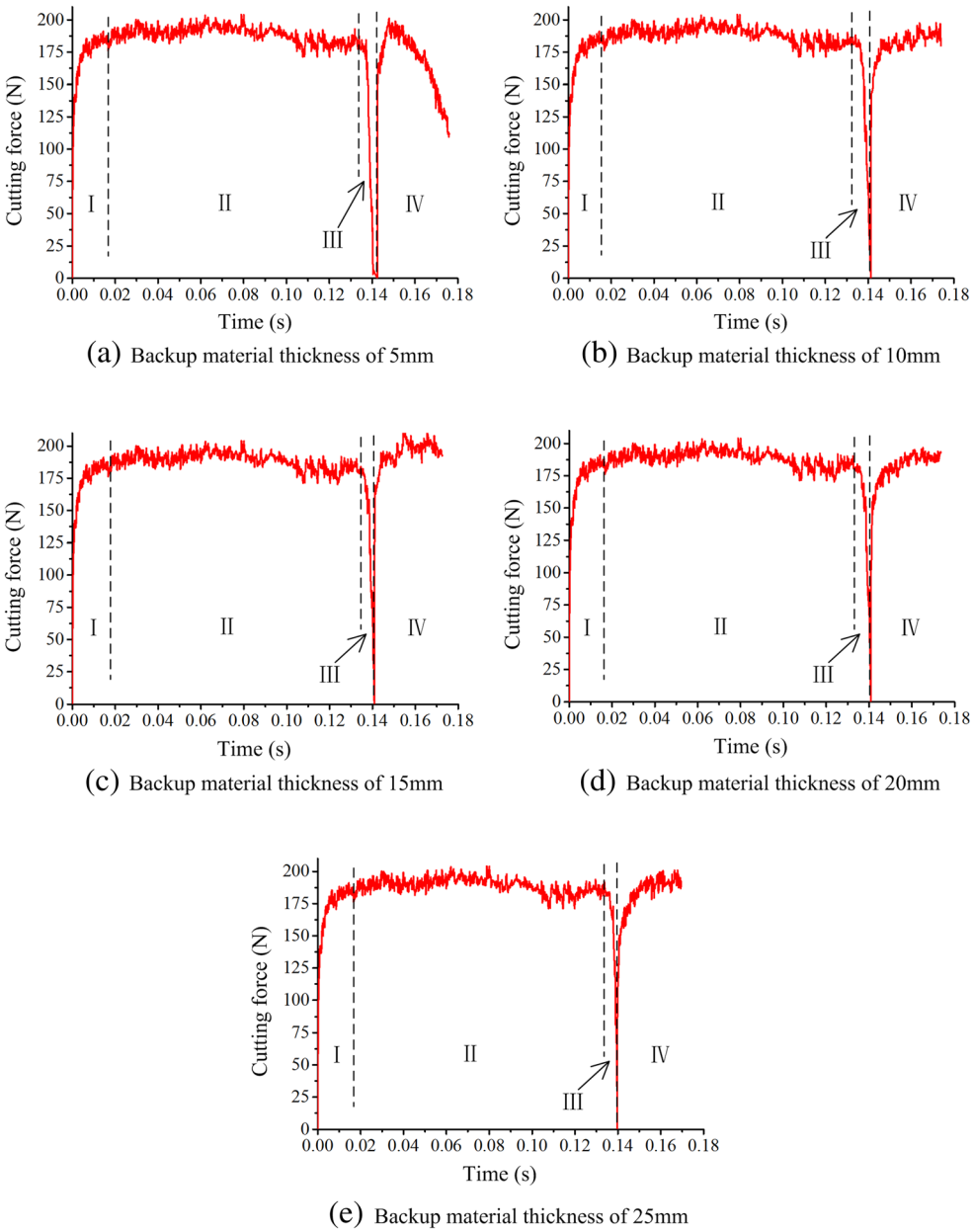


**Fig. 16** Cutting force curves under five different backup material thicknesses

state can reach a same value, about 188 N. Thus, it can be concluded that the steady-state cutting force is not affected by the thickness and height of the backup material. It is noted that cutting with a backup material would not cause a shock at tool nose or reduce tool life.

## 4 Conclusions

1. The formation of a negative burr includes eight stages: initial chip formation, steady state of chip formation, continuous cutting state, initiation of burr formation, pivoting state, initiation of crack, burr development and crack propagation, and final negative burr formation. In addition, the formation and stress variations of negative shear zone were considered to be the main reasons of negative burr formation.
2. The backup material thickness is an effective parameter to control burr sizes. The thinner the backup material is, the larger the burr size is. With the increase of backup material thickness, the support stiffness of backup material improved, and thus, the burr size reduced. However, when the support stiffness of backup material was high enough, increasing its thickness could become ineffective, and thus, excessively thick backup material is not recommended.
3. The backup material height is another effective parameter to control burr size, so as the burr profile. Negative burrs

could be formed with a smaller backup material height, while larger backup material height causes a material waste. Backup material height closed to zero could be the best choice for the present study.

4. The steady-state cutting forces are considered to have nothing to do with the backup material thickness, similarly the backup material height. This indicates that cutting with a backup material would not cause a shock at the tool nose or reduce tool life.

**Acknowledgments** This work was supported by the National Natural Science Foundation of China (51375174), Fundamental Research Funds for the Central Universities (2014ZG0004, 2015PT013), Guangdong Natural Science Funds for Distinguished Young Scholar (S2013050014163), and Zhujiang Science Technology New Stars Foundation (2011J2200066).

**Compliance with ethical standards**

**Conflict of interest** The authors declare that they have no conflict of interest.

## References

1. Ko SL, Chang JE, Yang GE (2003) Burr minimizing scheme in drilling. J Mater Process Technol 140(1):237–242
2. Toh CK (2007) The use of ultrasonic cavitation peening to improve micro-burr-free surfaces. Int J Adv Manuf Technol 31(7–8):688–693
3. Gillespie LK (1981) Deburring technology for improved manufacturing. SME, Dearborn
4. Takazawa K (1988) The challenge of burr technology and its worldwide trends. Bull Jpn Soc Precis Eng 22(3):165–170
5. Gillespie LK, Blotter PT (1976) The formation and properties of machining burrs. J Manuf Sci Eng (J Eng Ind) 98(1):66–74
6. Pekelharing AJ (1980) Cutting tool damage in interrupted cutting. Wear 62(1):37–48
7. Ko SL, Dornfeld DA (1991) A study on burr formation mechanism. J Eng Mater Technol 113(1):75–87
8. Chern GL (2006) Study on mechanisms of burr formation and edge breakout near the exit of orthogonal cutting. J Mater Process Technol 176(1):152–157
9. Toropov A, Ko SL, Kim BK (2005) Experimental study of burrs formed in feed direction when turning aluminum alloy al6061-t6. Int J Mach Tools Manuf 45(9):1015–1022
10. Toropov A, Ko SL (2006) A model of burr formation in the feed direction in turning. Int J Mach Tools Manuf 46(15):1913–1920
11. Toropov AA, Ko SL, Lee JM (2006) A new burr formation model for orthogonal cutting of ductile materials. CIRP Ann Manuf Technol 55(1):55–58
12. Segonds S, Masounave J, Songmene V, Bès C (2013) A simple analytical model for burr type prediction in drilling of ductile materials. J Mater Process Technol 213(6):971–977
13. Niknam SA, Songmene V (2013) Modeling of burr thickness in milling of ductile materials. Int J Adv Manuf Technol 66(9–12): 2029–2039
14. Chern GL (2006) Experimental observation and analysis of burr formation mechanisms in face milling of aluminum alloys. Int J Mach Tools Manuf 46(12):1517–1525
15. Lin TR (2000) Experimental study of burr formation and tool chipping in the face milling of stainless steel. J Mater Process Technol 108(1):12–20
16. Olvera O, Barrow G (1996) An experimental study of burr formation in square shoulder face milling. Int J Mach Tools Manuf 36(9): 1005–1020
17. Wyen CF, Jaeger D, Wegener K (2013) Influence of cutting edge radius on surface integrity and burr formation in milling titanium. Int J Adv Manuf Technol 67(1–4):589–599
18. Wu X, Li L, He N, Zhao M, Zhan Z (2015) Investigation on the influence of material microstructure on cutting force and bur formation in the micro cutting of copper. Int J Adv Manuf Technol 79(1–4):321–327
19. Parle D, Singh RK, Joshi SS, Ravikumar GVV (2014) Modeling of microcrack formation in orthogonal machining. Int J Mach Tools Manuf 80:18–29
20. Kountanya R, Al-Zkeri I, Altan T (2009) Effect of tool edge geometry and cutting conditions on experimental and simulated chip morphology in orthogonal hard turning of 100Cr6 steel. J Mater Process Technol 209(11):5068–5076
21. Buchkremer S, Klocke F, Lung D (2015) Finite-element-analysis of the relationship between chip geometry and stress triaxiality distribution in the chip breakage location of metal cutting operations. Simul Model Pract Theory 55:10–26
22. Guo YB, Dornfeld DA (2000) Finite element modeling of burr formation process in drilling 304 stainless steel. J Manuf Sci Eng 122(4):612–619
23. Saunders LKL (2003) A finite element model of exit burrs for drilling of metals. Finite Elem Anal Des 40(2):139–158
24. Long Y, Guo C (2012) Finite element modeling of burr formation in orthogonal cutting. Mach Sci Technol 16(3):321–336
25. Chen MJ, Ni HB, Wang ZJ, Jiang Y (2012) Research on the modeling of burr formation process in micro-ball end milling operation on Ti–6Al–4V. Int J Adv Manuf Technol 62(9–12):901–912
26. Park IW, Dornfeld DA (2000) A study of burr formation processes using the finite element method: part I. J Eng Mater Technol 122(2): 221–228
27. Deng WJ, Xia W, Tang Y (2009) Finite element simulation for burr formation near the exit of orthogonal cutting. Int J Adv Manuf Technol 43(9–10):1035–1045
28. Deng WJ, Xie ZC, Lin P, Xu TK (2012) Study on burr formation at the top edge in rectangular groove cutting. Adv Mater Sci Eng. doi: 10.1155/2012/956208
29. Wan ZP, Li YC, Tang HL, Deng WJ, Tang Y (2014) Characteristics and mechanism of top burr formation in slotting microchannels using arrayed thin slotting cutters. Precis Eng 38(1):28–35
30. Kilickap E (2010) Modeling and optimization of burr height in drilling of Al-7075 using Taguchi method and response surface methodology. Int J Adv Manuf Technol 49(9–12):911–923
31. Karnik SR, Gaitonde VN (2008) Development of artificial neural network models to study the effect of process parameters on burr size in drilling. Int J Adv Manuf Technol 39(5–6):439–453
32. Park IW, Dornfeld DA (2000) A study of burr formation processes using the finite element method: part ii—the influences of exit angle, rake angle, and backup material on burr formation processes. J Eng Mater Technol 122(2):229–237
33. Johnson GR, Cook WH (1985) Fracture characteristics of three metals subjected to various strains, strain rates, temperatures and pressures. Eng Fract Mech 21(1):31–48
34. Cockcroft MG, Latham DJ (1968) Ductility and the workability of metals. J Inst Metals 96(1):33–39
35. Oh SI, Chen CC, Kobayashi S (1979) Ductile fracture in axisymmetric extrusion and drawing—part 2: workability in extrusion and drawing. J Manuf Sci Eng 101(1):36–44